Optimisation of chemical solution deposition of Indium Tin Oxide thin films

Tor Olav Løveng Sunde [a,1], Mari-Ann Einarsrud [a] and Tor Grande [a,*]

[a] Department of Materials Science and Engineering,

Norwegian University of Science and Technology, N-7491 Trondheim, Norway

Abstract

An environmentally friendly aqueous sol-gel process has been optimised to deposit indium tin oxide (ITO) thin films, aiming to improve the film properties and reduce the deposition costs. It was demonstrated how parameters such as cation concentration and viscosity could be applied to modify the physical properties of the sol and thereby reduce the need for multiple coatings to yield films with sufficient conductivity. The conductivity of the thin films was enhanced by adjusting the heat treatment temperature and atmosphere. Both increasing the heat treatment temperature of the films from 530 to 800 °C and annealing in reducing atmosphere significantly improved the electrical conductivity, and conductivities close to the state of the art sputtered ITO films were obtained. A pronounced decreased conductivity was observed after exposing the thin films to air and the thermal reduction and ageing of the film was studied by in situ conductivity measurements.

[*] *Corresponding author. E-mail, grande@ntnu.no*, phone +47 73594084, fax: +47 73550203

[1] Present address: SINTEF Materials and Chemistry, Forskningsveien 1, 0314 Oslo, Norway.

1. Introduction

Transparent conducting oxides (TCOs) demonstrate the unique combination of having a near-metallic electrical conductivity and being transparent in the visible region of the spectrum. TCOs have therefore found numerous technological applications, such as flat panel displays, photovoltaic devices, light emitting diodes and gas sensors [1-4]. Indium oxide doped with tin oxide, referred to as Indium Tin Oxide (ITO) is often recognised as the TCO with the superior combination of properties and is therefore widely used for many of the applications [5-8]. ITO thin films can be deposited by a variety of techniques, such as sputtering, pulsed laser deposition, chemical vapour deposition and vacuum evaporation, with sputtering being the most widely used industrially [1-8]. On the other hand, wet chemical methods offers many advantages compared to the physical deposition techniques, such as cost, simplicity and readily control of homogeneity and composition, combined with no need for vacuum in the deposition chamber [9-11]. Water and organic liquids can both be used as solvents for wet chemical synthesis, but the organic solvents are often flammable, expensive or harmful to the environment, and aqueous solution processing is therefore potentially more suitable for industrial processes [12]. The majority of the reported wet chemical methods for depositing ITO are based on organic solvents like ethylene glycol, ethanol or acetylacetone [13-16], although some water based processes have been reported [12, 17-19]. In several of these cases chlorides are used as the chemical precursor, where the removal of residual chlorides can complicate the process.

We have recently developed an environmentally friendly aqueous sol-gel route to ITO thin films [20]. The method is a modified Pechini process [21] using simple and inexpensive precursors, which also circumvents the challenges related to the use of chlorides. The specific resistance of these films was demonstrated to be about $4.6 \cdot 10^{-3}$ Ωcm which show the potential of the method, but calls for further optimization in order to match the conductivity of

sputtered ITO thin films [6]. Here we report on the optimisation of the chemical solution deposition process. The synthesis was modified in order to control the thickness of the deposited layer, the viscosity of the sol was characterized and the thermal decomposition/crystallization of the prepared gel was further analysed. Deposition on single crystalline substrates is also reported. Finally, the annealing temperature and atmosphere was further optimized in order to enhance the electrical conductivity. In situ characterization of the electrical conductivity of the films was performed during the thermal annealing.

2. Experimental

2.1. Sample preparation

The deposition of the thin films from the sol-gel process is described in detail elsewhere [20]. Indium (III) nitrate hydrate ($In(NO_3)_3 \cdot xH_2O$, 99.9 %, Aldrich) and tin (II) acetate ($Sn(CH_3CO_2)_2$, 99.9 %, Aldrich) were used as precursors, with a tin doping amount of 10 cation% (cat%). Acetic acid (p.a. Acros Organics) and ethylene glycol ($C_2H_4(OH)_2$, VWR) were used as complexing agents, with a molar ratio between the cations in the solution and each of the organic additives of 1:1.5. Stoichiometric amounts of the cation precursors and organic complexing agents were dissolved in deionized water, and solutions with cation concentrations of 0.4 or 1.0 M were prepared. These solutions were mixed in a 1:1 volume ratio with a solution of de-ionized water with either 3 or 5 wt% polyvinyl alcohol (PVA, VWR, average $M_w \approx 88000$ g/mol), utilised as a wetting agent, giving a final cation concentration in the solutions used for spin coating of 0.2 or 0.5 M. Four different solutions were used, with different cation concentrations and PVA content as labelled in Table 1. The cation concentration is the final concentration after mixing of the solutions, while the PVA content is the content in the PVA solution before mixing. The films that were used to optimise

the conductivity were all prepared from Solution 1, in order to be comparable with the previous work.

The thin films were deposited by spin coating on polished square single-crystalline <100> YSZ, <0001> Al_2O_3 and <100> MgO substrates (MolTech GmbH) of 15 x 15 mm and on glass substrates (Menzel-Gläser, microscope slides) of 25 x 25 mm. After the solution was applied to the substrates they were spun at 3000 rpm for 45 s (Laurell WS-400B-6NPP-Lite Spinner). The films were calcined under vacuum (1 Pa) in a rapid thermal process furnace (RTP, Jipelec JetFirst 200 Processor) at 530 or 600 °C for 1 h or at 700 or 800 °C for 30 min. This procedure was repeated two times in order to make films with three deposited layers. After about two weeks of storage in ambient conditions some of the films were annealed in 5 % hydrogen in argon for 10 h at 400 °C.

Corresponding gels were prepared by dissolving stoichiometric amounts of the precursors and complexing agents and evaporating the solvent. For the gels, tartaric acid (ReagentPlus ≥99 %, Sigma-Aldrich) and ethylene glycol were used as complexing agents, and the amount of tin was 5 cation%.

2.2. Characterisation

The electrical properties of the thin films were measured using an in-house built van der Pauw apparatus with platinum contacts. The sheet resistance at ambient conditions was obtained by performing eight different measurements on each film, where the current and voltage drop was measured along different sides of the films and in different directions. The sheet resistance, R_s, was calculated by Equation 1 [22]:

$$R_s = \frac{\pi}{\ln 2} * \frac{R_{horizontal} + R_{vertical}}{2} * f \qquad (1)$$

where the resistances, $R_{horizontal}$ and $R_{vertical}$, were determined as the average of the first and last four measurements respectively and f is a correction factor obtained from Equation 2 [22]:

$$\frac{R_{horizontal} - R_{vertical}}{R_{horizontal} + R_{vertical}} = \frac{f}{\ln 2} * \operatorname{arccosh} \frac{e^{\frac{\ln 2}{f}}}{2} \quad (2)$$

The sheet resistance is the specific resistance of the material, ρ, divided by the thickness of the film, t, as shown in Equation 3:

$$R_s = \frac{\rho}{t} \quad (3)$$

In situ conductivity during and after annealing in 5 % H_2 in Ar was measured by placing the sample inside a quartz tube in a furnace. A gas flow of about 50 mL/min was applied. The heating and cooling rates were 200 K/h. The sheet conductivity in the in situ measurements was calculated from the current and voltage drop in the van der Pauw set-up, which corresponds to the inverse of either $R_{horizontal}$ or $R_{vertical}$ in Equation 1. This value should not be mistaken for the real sheet conductivity of the film, which generally would be about a factor of $\pi/\ln(2)$ lower.

X-ray diffraction (XRD) was performed on the thin films with a Siemens D5005 with a gracing incidence angle set-up, Cu-radiation source ($CuK\alpha_{1,2}$), Göbel mirror, equatorial soller slits on the detector side and a Scintillation detector. The incident angle was 2 °, and the films were analysed from 20 to 70 °, with an incremental step of 0.08 ° and a counting time of 7.3 s per step. Rietveld refinements of the diffractograms were carried out using the Topas software, v4.2 and the space group $Ia\bar{3}$ [23] in order to obtain the lattice parameter and the crystallite size by the line broadening.

Scanning electron microscopy (FEG-SEM, Zeiss Ultra 55 Limited Edition) was performed on the top view of the film surfaces.

The viscosity of prepared solutions was measured with a Thermo Scientific HAAKE Mars III rheometer using the RheoWin 4 software. The experiments were performed at 25 °C. The reported values for the viscosity were obtained at a shear rate of 500 s^{-1}.

The thermal behaviour of the prepared gels was analysed by a thermogravimetrical analysis (TGA, Netzsch, STA 449 C) up to 800 °C in air, with a heating rate of 2 K/min. Differential scanning calorimetry (DSC) was also performed in the same experiment**.** A Netzsch, QMS 403 Aëolos mass spectrometer (MS) was attached to analyse the evolved gases.

3. Results

3.1. Effect of different substrates and modifying the spin coating solution

The thickness of each deposited layer from Solution 1 was ~17 nm as previously reported [20], which means that multiple depositions is required to achieve sufficient conductivity. An optimization of the process was performed in order to control the thickness of the deposited layers. An important parameter during spin coating is the viscosity of the solution [24, 25], and the measured viscosity of selected solutions is summarised in Table 2. The amount of PVA clearly had a dramatic effect on the viscosity. Increasing the cation concentration in the solution was also observed to increase the viscosity as the ratio between cations and complexing agents was kept constant for all solutions. The solutions demonstrated Newtonian behaviour, as illustrated in Figure 1 (a), except for the 10 wt% PVA solution which exhibited shear thinning properties, as shown in Figure 1 (b). In the first case the viscosity quickly reached a stable value as the shear rate was increased, whereas the viscosity was observed to be reduced as the shear rate increased in the latter.

The sheet resistance of films deposited on glass, YSZ and Al_2O_3 from Solution 1 and heat treated at 530 °C was 803, 630 and 558 Ω/□ respectively, see Figure 2. Deposition of films on

the MgO substrate was not successful. Following this, solutions with different PVA content and cation concentrations were used to deposit ITO thin films on Al_2O_3 substrates and heat treated at 600 °C to complete the removal of carbon residues by combustion. The solutions labelled Solution 1 to 4, produced films with sheet resistance of 1191, 221, 248 and 131 Ω/□, respectively, as shown in Figure 2. The conductivity of these films is also summarized in Table 2. These thin films were demonstrated by XRD to be nano-crystalline and phase pure after the heat treatment, with the cubic In_2O_3 bixbyite crystal structure (space group $Ia\bar{3}$, #206), as shown for the film on YSZ presented in Figure 3.

3.2. Thermal decomposition of the gel

Amorphous gels were formed after evaporation of the solvent from the precursor solution, showing that no precipitations had occurred and pointing towards formation of homogeneous gels. The gels decomposed and crystallised to the desired final oxide product upon calcination, confirming previous findings [20]. TGA/MS analysis of a gel prepared with tartaric acid and ethylene glycol is given in Figure 4. The onset of the major weight loss occurred above 100 °C and the weight saturated at around 600 °C. From 100-200 °C evaporation of H_2O from the gel is evident (Fig. 4b), but there are still signs of water being evaporated at temperatures up to 500 °C. The signals from CO_2 as well as NO and NO_2, displayed in Figure 4 (c) and (d) respectively, demonstrates the removal of organics and nitrates from the gel. In the DSC exothermic peaks due to the oxidation and decomposition of the organic and nitrate components are visible in the same temperature region where the mass loss is evident. The exothermic decomposition released sufficient amount of heat to induce crystallization of the remaining oxide. We have previously observed that SnO_2 is precipitating when similar ITO materials with 5 cat% Sn were heat treated at 1000 °C, but not at 800 °C and lower temperatures [26]. No traces of SnO_2 were observed by XRD after the TGA

experiments, pointing to the local temperature during the decomposition being sufficiently below 1000 °C.

3.3. Optimisation of the conductivity

The sheet resistance of ITO thin films on YSZ substrates heat treated at temperatures ranging from 530 to 800 °C measured after different steps of the fabrication is given in Table 3 and Figure 5. Two films were prepared for each temperature and one of them subsequently annealed. Data are presented for the films directly after deposition, before and directly after reduction with 5 % H_2 and after two weeks storage after reduction. Increasing the heat treatment temperature after film deposition had a significant effect on the conductivity of the films. The sheet resistance decreased from 520 Ω/□ for the film heat treated at 530 °C to 353 Ω/□ for the one treated at 800 °C. The sheet resistance of two films prepared at the same conditions was within 5 % of each other, demonstrating the reproducibility of the aqueous sol-gel deposition process. Furthermore, when the sheet resistance was re-measured before the annealing in reducing atmosphere, the sheet resistance was shown to decrease from 7 to 16 %, demonstrating an ageing effect. No trend could be observed between the size of this effect and the heat treatment temperature. XRD was performed after the different steps in the process and all of the films appeared nano-crystalline and phase pure, similar to the diffractogram shown in Figure 3. All of the films also appeared visually transparent, but no further optical characterisation was performed.

The in situ sheet conductivity for the four films measured during annealing in reducing atmosphere is given in Figure 6. The initial conductivity reflects that the conductivity was improved by increasing the initial heat treatment temperature, as shown in Table 3 and Figure 5. The conductivity of all of the films initially increased with increasing temperature, in line with expectations for semiconductor materials. When the temperature reached about 400 °C the contact with the platinum electrodes appeared to be damaged, causing noise. However, the

conductivity reached a stable value during the 10 h annealing, which we interpret as the equilibrium conductivity. The conductivity was lowered during the cooling, but stabilised at a level of 55 to 64 % higher than the initial conductivity prior to the heat treatment. When other films were annealed in more oxidising atmospheres, like air or nitrogen, the opposite effect was observed, namely a lower conductivity after the annealing.

The conductivity of the films stabilized after cooling and in the stagnant 5 % H_2 gas, but the conductivity immediately decreased when the films were exposed to air. The sheet conductivity of a film at ambient conditions directly after exposure to air was measured over a period of two days and is displayed in Figure 7. Initially, there is a drastic decrease in the conductivity. Already within the first minute the conductivity decreased 2 %, and the conductivity was further lowered by 5 and 10 % after 6 and 24 minutes. The reduction in conductivity stabilised after about 14 hours. The sheet resistance stabilised at 18 to 27 % higher values after about two days. The values given in Table 3 and Figure 5 were measured directly after exposure to air and two days later. When the sheet resistances were measured again 3 months after the reduction, the values had further increased with an average of approximately 3 %. The sheet resistance of the films which had not been annealed in reducing atmosphere, on the other hand, had on average decreased with 6 % after 3 months of storage, probably pointing towards the same ageing phenomenon as mentioned above.

The lattice parameters of the films measured by XRD before and after the reduction are given in Table 4 and Figure 8. Film 1 and Film 2 were prepared at the same conditions, but only Film 1 was reduced. Two significant trends could be observed. First, the films heat treated at lower temperatures had significantly larger lattice parameters than powders of the same composition, pointing towards tensional strain in the films. The strain appears to be released, thereby relaxing the lattice parameter, when the heat treatment temperature was increased above 530 °C. Second, reduction of the films increased the lattice parameter with about 0.002

Å for all temperatures. Though this latter effect is comparable in size with the estimated uncertainty, the small increase was consistent and in good agreement with the change in lattice parameter of ITO thin films due to reduction [27]. The lattice parameter of the two films heat treated at each temperature was in reasonable agreement. The crystallite size of the films calculated from the line broadening of their diffractograms is given in Table 4 and Figure 9. Increasing the annealing temperature did not increase the crystallite size significantly, showing that the crystallinity or grain size of the films was not altered due to the thermal annealing. This is in good accordance with results obtained from studying the sintering process of nano-crystalline ITO powders [26], where it was confirmed that the grain growth of ITO at temperatures below 800 °C was minor. The reduction did not appear to affect the grain size in the films, in line with expectations.

SEM micrographs of the thin films are given in Figure 10. It was confirmed that the films appeared homogeneous and that the microstructure was similar for the films heat treated at different temperatures. The grain size was 20 to 30 nm for all the films, and it was not possible to observe a significant increase in the grain size with increasing heat treatment temperature, correlating well with the crystallite sizes from XRD. The microstructure of the films after the reduction was similar to the ones given in Figure 10.

4. Discussion

4.1. Electrical conductivity

The improvement of the conductivity of ITO thin films by annealing at different temperatures and atmospheres has previously been discussed [12-14, 28, 29]. The present work also demonstrates that both increasing the heat treatment temperature and annealing in reducing atmospheres significantly improved the conductivity of the films. The thickness of the films

in this work was not determined. However, the spin coating process was similar to our initial study [20], which yielded a thickness of 17 nm per deposition (solution 1) with a high reproducibility. The optimised stable sheet resistance obtained in this work is 131 Ω/□. The stable specific resistance after reduction of the film heat treated at 800 °C is estimated to 7 ± $1 \cdot 10^{-4}$ Ω·cm using an estimate of the film thickness from our previous work. This value is excellent compared to other ITO thin films prepared by aqueous sol-gel methods and comparable to the best reported values for ITO. The reproducibility of the deposition process was also demonstrated to be excellent, especially for films deposited from the same batch of solutions.

The conductivity of the films increased by 55-64 % due to the annealing in 5 % H_2 in Ar. This improvement can be explained by the point defect chemistry of ITO, which is illustrated by the following Kröger-Vink equation [27]:

$$(2\ Sn_{In}^{\bullet} O_i'')^{X} \rightarrow \tfrac{1}{2}\ O_2\ (g) + 2\ Sn_{In}^{\bullet} + 2e' \qquad (4)$$

Oxygen interstitials in the lattice will form neutral clusters with the n-type tin donor atoms and compensate and trap some of the itinerant electrons [27]. Annealing in reducing atmospheres can thereby increase the conductivity by removing oxygen interstitials. It was also demonstrated that annealing in oxidizing atmospheres decreased the conductivity, which further point to the importance of the redox reaction (Equation 4). Furthermore, the thin film heat treated at 800 °C possessed a sheet resistance between 32 and 47 % lower than the film annealed at 530 °C after the different processing steps (Table 3). The improvement of the conductivity by the higher annealing temperature is not as straightforward to explain. As the thickness of the films should not change (no major change in microstructure), it is proposed that the decrease in the sheet resistance is caused by a lowering of the specific resistivity of the films. Our previous work demonstrated that the microstructure of the films consisted of

individual layers from each deposition and that the adhesion between the layers appeared to be weaker than the bond between the grains in each layer [20]. Annealing at higher temperatures could, thereby, increase the conductivity by strengthening the physical contact between the layers. A significant amount of tensional strain present in the films was released by increasing the heat treatment temperature (Figure 8), which probably affect the conductivity**.** Furthermore, it is also demonstrated that crystallite size of the films did not increase significantly by the increased temperature. Tahar et al. have calculated a carrier mean free path of 1.6 nm for ITO with 10 cat% Sn [30], which suggests that the grain sizes in the films are sufficiently large to avoid grain boundary scattering causing significant reduction of the mobility. Though the effect of the increased crystallite size may be small, it cannot be ruled out. The crystallinity of the films could also be improved by the increased temperature, although the diffraction data did not demonstrate a significant change. It is not clear which of the aforementioned effects is the most important regarding the improved conductivity of the films that were heat treated at higher temperatures. Regardless of the heat treatment temperature and the initial conductivity before reduction, all of the films experienced a decrease in the sheet resistance of about 50 % after the 10 h annealing in 5% H_2 in Ar. This implies that the improvement of conductivity due to the increased temperature and the reducing atmosphere are two separate effects which can be utilized independently.

It was clearly demonstrated that the conductivity of the films which had been annealed in reducing atmospheres decreased when the films were exposed to air (Figure 7). Similar observations have been reported for thin films prepared from dispersions of nano-sized ITO particles [31-33]. In these cases the long term decrease of the conductivity during storage in air for several weeks was proposed to be due to incorporation of oxygen into the lattice and re-oxidation of the films. However, the initial in situ response to the conductivity after exposure to air was not characterised. The electrical response of ITO to different atmospheres

is complicated and can be caused by both bulk and surface effects [34-37]. It is well known that oxygen and water from the air will chemisorb to the ITO surface immediately after exposure to ambient conditions and influence its conductivity [38, 39]**.** While adsorbed oxygen will extract electrons from the semiconductor and decrease its conductivity, adsorbed water will have the opposite effect [34, 35, 40]. As the conductivity in the present case was demonstrated to decrease, the response could not have been caused by chemisorption of water. It is well known that oxygen chemisorption on ITO surfaces is active at room temperature [37]. Though there was a dramatic decrease in the conductivity the first minutes after exposure to air, the conductivity also slowly decreased during storage in air several weeks after the reduction. It has been observed that adsorbed surface oxygen can diffuse into the lattice and re-oxidize ITO even at relatively low temperatures, however this re-oxidized layer is only proposed to be a few Å thick [36, 37, 41]. Diffusion of oxygen in bulk In_2O_3 is slow already at 800 °C [42, 43]. Even though the bulk oxygen diffusion is slow at room temperature, grain boundary diffusion may enhance the kinetics in nano-crystalline ITO [44]. Porosity in the thin film may also contribute to faster oxidation kinetics. We propose that the initial decrease in conductivity as a response to the exposure to ambient air is caused by chemisorption of oxygen on the surface of the ITO thin films, and that oxygen also diffuses into the thin films and decreases the conductivity by re-oxidation over time.

It was observed that the sheet resistance of the films decreased with 7 to 16 % within two weeks after their deposition and heat treatment in 1 Pa pressure. It is possible that this was caused by chemisorption of water on the surface, which would increase the conductivity of the films, as described above. However, this process is rapid and it has been reported that the XPS signal from the water adsorption gains most of its intensity within seconds and minutes after exposure to air, and that only a limited increase is observed during prolonged exposure [38]. It is therefore reasonable to assume that most of the water adsorption would already

have occurred before the initial sheet resistance measurement, conducted a couple of hours after the heat treatment. This effect can therefore not explain the significant decrease after longer storage in air. On the other hand, it is possible that this observation is caused by some sort of ageing or relaxation of the films, however further investigations would be necessary in order to conclude regarding the cause of this effect.

4.2. Effect of different substrates and modifying the spin coating solution

In order to increase the thickness of the deposited layers the cation concentration and PVA content in the spin coating solutions were altered. Increasing the PVA content in the solutions was demonstrated to increase the viscosity of the solutions (Table 2), which thereby increases the thickness of the liquid film formed during spinning [25, 45]. Increasing the cation concentration further increased the viscosity, and the thickness of the final oxide layer formed from a liquid film will also increase linearly with the cation concentration [46]. It was clearly demonstrated how both the cation concentration and viscosity influences the sheet resistance of the four films prepared from the different solutions (Table 2 and Figure 2). Though the true thickness of the films was not confirmed, it is proposed that this is caused by differences in film thickness and to a much lesser extent by changes in the specific resistance of the films, which also could affect the sheet resistance (Equation 3). The four films were heat treated at the same temperature and although the different amounts of organics and nitrates could cause an increase in the local temperature during oxidation, it is reasonable that the specific resistance of the films should be fairly equal. Hence, the choice of the cation concentration and PVA content can be used to tailor the thickness of the film to the desired application. For comparison, the sheet resistance of the thin film prepared by three coatings of Solution 4 (131 Ω/□) is significantly lower than a film prepared by ten depositions of Solution 1 in our

previous work (270 Ω/□) [20]. Moreover, it was demonstrated that a too high viscosity can lead to shear thinning of the solution, which would make it difficult to obtain a homogeneous film thickness after spinning. If the film is over a certain thickness it might also be more prone to cracking [24], and the deposition parameters should be carefully optimised for the specific case.

Finally, the different substrates appeared to influence on the sheet resistance of the films (Table 2 and Figure 2). The films deposited on YSZ and Al_2O_3 substrates had slightly lower sheet resistances than a similar film deposited on glass, while no film was formed on MgO, the substrate with the most basic properties. This indicates that the interaction between the substrate and solution is important. It is proposed that differences in surface tension caused a poor wetting of the solution on MgO, and also influenced the thickness of the formed films for the other substrates.

5. Conclusions

An inexpensive and environmentally friendly aqueous sol-gel process has been further optimised to yield ITO thin films with excellent electrical properties. Furthermore, the cation concentration and viscosity of the spin coating solutions were modified in order to control the thickness of the deposited layers. By increasing the heat treatment temperature to 800 °C and annealing in 5 % H_2 in Ar, films with conductivity close to the best reported values for ITO was prepared. Furthermore, in situ conductivity measurements were performed in order to analyse the effect of the atmosphere during different steps in the process. The reducing annealing was demonstrated to improve the conductivity, but the conductivity decreased after exposure to air after the annealing and the possible causes of the different observations was discussed.

Acknowledgement

Financial support from NTNU and access to the clean room facilities at NTNU NanoLab are acknowledged.

References

[1] D.S. Ginley, C. Bright, Transparent conducting oxides, MRS Bull. 25 (2000) 15-18.

[2] K.L. Chopra, S. Major, D.K. Pandya, Transparent conductors - A status review, Thin Solid Films 102 (1983) 1-46.

[3] T.J. Coutts, D.L. Young, X.N. Li, Characterization of transparent conducting oxides, MRS Bull. 25 (2000) 58-65.

[4] B.G. Lewis, D.C. Paine, Applications and processing of transparent conducting oxides, MRS Bull. 25 (2000) 22-27.

[5] I. Hamberg, C.G. Granqvist, Evaporated Sn-doped In_2O_3 films - Basic optical properties and applications to energy-efficient windows, J. Appl. Phys. 60 (1986) R123-R159.

[6] C.G. Granqvist, A. Hultaker, Transparent and conducting ITO films: new developments and applications, Thin Solid Films 411 (2002) 1-5.

[7] R.B.H. Tahar, T. Ban, Y. Ohya, Y. Takahashi, Tin doped indium oxide thin films: Electrical properties, J. Appl. Phys. 83 (1998) 2631-2645.

[8] E.N. Dattoli, W. Lu, ITO nanowires and nanoparticles for transparent films, MRS Bull. 36 (2011) 782-788.

[9] D.S. Hecht, R.B. Kaner, Solution-processed transparent electrodes, MRS Bull. 36 (2011) 749-755.

[10] M. Kakihana, M. Yoshimura, Synthesis and characteristics of complex multicomponent oxides prepared by polymer complex method, Bull. Chem. Soc. Jpn. 72 (1999) 1427-1443.

[11] R.M. Pasquarelli, D.S. Ginley, R. O'Hayre, Solution processing of transparent conductors: from flask to film, Chem. Soc. Rev. 40 (2011) 5406-5441.

[12] R.B.H. Tahar, T. Ban, Y. Ohya, Y. Takahashi, Optical, structural, and electrical properties of indium oxide thin films prepared by the sol-gel method, J. Appl. Phys. 82 (1997) 865-870.

[13] Y. Takahashi, S. Okada, R.B.H. Tahar, K. Nakano, T. Ban, Y. Ohya, Dip-coating of ITO films, J. Non-cryst. Sol. 218 (1997) 129-134.

[14] S.S. Kim, S.Y. Choi, C.G. Park, H.W. Jin, Transparent conductive ITO thin films through the sol-gel process using metal salts, Thin Solid Films 347 (1999) 155-160.

[15] K. Daoudi, B. Canut, M.G. Blanchin, C.S. Sandu, V.S. Teodorescu, J.A. Roger, Densification of In_2O_3:Sn multilayered films elaborated by the dip-coating sol-gel route, Thin Solid Films 445 (2003) 20-25.

[16] D. Gallagher, F. Scanlan, R. Houriet, H.J. Mathieu, T.A. Ring, Indium Tin Oxide thin-films by metal-organic decomposition, J. Mater. Res. 8 (1993) 3135-3144.

[17] C. Legnani, S.A.M. Lima, H.H.S. Oliveira, W.G. Quirino, R. Machado, R.M.B. Santos, M.R. Davolos, C.A. Achete, M. Cremona, Indium tin oxide films prepared via wet chemical route, Thin Solid Films 516 (2007) 193-197.

[18] S. Kundu, P.K. Biswas, Synthesis and photoluminescence property of nanostructured sol-gel indium tin oxide film on glass, Chem. Phys. Lett. 414 (2005) 107-110.

[19] B. Schumm, P. Wollmann, J. Fritsch, J. Grothe, S. Kaskel, Nanoimprint patterning of thin cadmium stannate films using a polymeric precursor route, J. Mater. Chem. 21 (2011) 10697-10704.

[20] T.O.L. Sunde, E. Garskaite, B. Otter, H.E. Fossheim, R. Saeterli, R. Holmestad, M.A. Einarsrud, T. Grande, Transparent and conducting ITO thin films by spin coating of an aqueous precursor solution, J. Mater. Chem. 22 (2012) 15740-15749.

[21] M. Pechini. Method of preparing lead and alkaline earth titanates and niobates and coating method using the same to form a capacitor, US Patent 3330697 (1967).

[22] L.J. van der Pauw, A method of measuring resistivity and Hall coefficient on lamellae of arbitrary shape, Philips Tech. Rev. 20 (1958) 220 - 224.

[23] M. Marezio, Refinement of crystal structure of In_2O_3 at 2 wavelengths, Acta Crystallogr. 20 (1966) 723.

[24] C.J. Brinker, A.J. Hurd, P.R. Schunk, G.C. Frye, C.S. Ashley, Review of sol-gel thin-film formation, 6th International workshop on glasses and ceramics from gels, (1992).

[25] D.E. Bornside, C.W. Macosko, L.E. Scriven, Spin coating - One-dimensional model, J. Appl. Phys. 66 (1989) 5185-5193.

[26] T.O.L. Sunde, M.A. Einarsrud, T. Grande, Solid state sintering of nano-crystalline indium tin oxide, J. Eur. Ceram. Soc. 33 (2013) 565-574.

[27] G. Frank, H. Kostlin, Electrical properties and defect model of tin-doped indium oxide layers, Appl. Phys. A 27 (1982) 197-206.

[28] T. Kanbara, M. Nagasaka, T. Yamamoto, Preparation of electrically conducting indium tin oxide thin-films by heat-treatment of mixed-metal hydroxide dispersion containing polymer binder, Chem. Mat. 2 (1990) 643-645.

[29] R. Balasundaraprabhu, E.V. Monakhov, N. Muthukumarasamy, O. Nilsen, B.G. Svensson, Effect of heat treatment on ITO film properties and ITO/p-Si interface, Mater. Chem. Phys. 114 (2009) 425-429.

[30] R.B.H. Tahar, T. Ban, Y. Ohya, Y. Takahashi, Electronic transport in tin-doped indium oxide thin films prepared by sol-gel technique, J. Appl. Phys. 83 (1998) 2139-2141.

[31] J. Ederth, A. Hultaker, P. Heszler, G.A. Niklasson, C.G. Granqvist, A. van Doorn, C. van Haag, M.J. Jongerius, D. Burgard, Electrical and optical properties of thin films prepared by spin coating a dispersion of nano-sized tin-doped indium oxide particles, Smart Mater. Struct. 11 (2002) 675-678.

[32] M. Mahajeri, A. Schneider, M. Baum, T. Rechtenwald, M. Voigt, M. Schmidt, W. Peukert, Production of dispersions with small particle size from commercial indium tin oxide powder for the deposition of highly conductive and transparent films, Thin Solid Films 520 (2012) 5741-5745.

[33] J. Puetz, M.A. Aegerter, Direct gravure printing of indium tin oxide nanoparticle patterns on polymer foils, Thin Solid Films 516 (2008) 4495-4501.

[34] M.J. Madou, S.R. Morrison, Chemical Sensing with Solid State Devices, 1st ed., Academic Press, Inc, San Diego, 1989.

[35] M. Batzill, U. Diebold, Surface studies of gas sensing metal oxides, Phys. Chem. Chem. Phys. 9 (2007) 2307-2318.

[36] G. Korotcenkov, V. Brinzari, J.R. Stetter, I. Blinov, V. Blaja, The nature of processes controlling the kinetics of indium oxide-based thin film gas sensor response, Sens. Actuator B-Chem. 128 (2007) 51-63.

[37] G. Korotcenkov, M. Ivanov, I. Blinov, J.R. Stetter, Kinetics of indium oxide-based thin film gas sensor response: The role of "redox" and adsorption/desorption processes in gas sensing effects, Thin Solid Films 515 (2007) 3987-3996.

[38] M. Brumbach, P.A. Veneman, F.S. Marrikar, T. Schulmeyer, A. Simmonds, W. Xia, P. Lee, N.R. Armstrong, Surface composition and electrical and electrochemical properties of freshly deposited and acid-etched indium tin oxide electrodes, Langmuir 23 (2007) 11089-11099.

[39] C.G. Zhou, J.Y. Li, S. Chen, J.P. Wu, K.R. Heier, H.S. Cheng, First-principles study on water and oxygen adsorption on surfaces of indium oxide and indium tin oxide nanoparticles, J. Phys. Chem. C 112 (2008) 14015-14020.

[40] N. Barsan, U. Weimar, Conduction model of metal oxide gas sensors, J. Electroceram. 7 (2001) 143-167.

[41] V. Brinzari, G. Korotcenkov, V. Matolin, Synchrotron radiation photoemission study of indium oxide surface prepared by spray pyrolysis method, Appl. Surf. Sci. 243 (2005) 335-344.

[42] J.H.W. Dewit, G. Vanunen, M. Lahey, Electron-concentration and mobility in In_2O_3, J. Phys. Chem. Sol. 38 (1977) 819-824.

[43] Y. Ikuma, T. Murakami, Oxygen tracer diffusion in polycrystalline In2O3, J. Electrochem. Soc. 143 (1996) 2698-2702.

[44] T. Grande, J.R. Tolchard, S.M. Selbach, Anisotropic Thermal and Chemical Expansion in Sr-Substituted LaMnO3+delta: Implications for Chemical Strain Relaxation, Chem. Mat. 24 (2012) 338-345.

[45] O. Yamamoto, T. Sasamoto, M. Inagaki, Indium tin oxide thin-films prepared by thermal decomposition of ethylene-glycol solution, J. Mater. Res. 7 (1992) 2488-2491.

[46] Q. Wei, H.X. Zheng, Y.H. Huang, Direct patterning ITO transparent conductive coatings, Sol. Eng. Mater. Sol. Cells 68 (2001) 383-390.

Tables and figures

Table 1. Label, PVA content and cation concentration of different solutions used for spin coating.

Solution label	PVA content [wt %]	Cation concentration [M]
Solution 1	3	0.2
Solution 2	3	0.5
Solution 3	5	0.2
Solution 4	5	0.5

Table 2. The viscosity of selected solutions with varying PVA content and cation concentration and the sheet resistance of ITO thin films prepared from the different solutions. The estimated uncertainty is ± 2 % for the viscosity and ± 1 % for the sheet resistance.

Solution	PVA content [wt%]	Cation concentration [M]	Viscosity [Pa · s]	Sheet resistance [Ω/□]
Distilled water	-	-	$9.06 \cdot 10^{-4}$	
Solution 1	3	0.2	$2.50 \cdot 10^{-3}$	1191
Solution 2	3	0.5	$3.65 \cdot 10^{-3}$	221
Solution 3	5	0.2	$7.92 \cdot 10^{-3}$	248
Solution 4	5	0.5	$9.49 \cdot 10^{-}3$	131
3 wt% PVA	3	-	$1.23 \cdot 10^{-2}$	
5 wt% PVA	5	-	$4.93 \cdot 10^{-2}$	
10 wt% PVA	10	-	1.01	

Table 3. The sheet resistance, R_s, after deposition, before the reduction, directly after reduction and two days after the reduction for ITO thin films deposited on YSZ. The estimated uncertainty of the values is 2 %.

Heat treatment temperature [°C]	R_s after deposition [Ω/□]	R_s before reduction [Ω/□]	R_s directly after reduction [Ω/□]	R_s two days after reduction [Ω/□]
530	520	469	201	242
530	523			
600	399	365	154	197
600	424			
700	350	301	128	156
700	343			
800†	353	295		128
800	354			

† The sheet resistance of the film which was heat treated at 800 °C was not measured directly after reduction.

Table 4. Cubic lattice parameter and crystallite size of films deposited on YSZ substrates and heat treated at different temperatures before and after reduction for 10 h at 400 °C in 5 % hydrogen in argon. The estimated uncertainty is ± 0.002 Å for the lattice parameter and ± 0.2 nm for the crystallite size.

Heat treatment temperature [°C]	Lattice parameter [Å]		Crystallite size [nm]	
	Before	After	Before	After
530	10.154	10.157	12.3	12.1
530	10.156		12.2	
600	10.143	10.144	13.0	12.7
600	10.138		12.7	
700	10.122	10.125	12.8	12.8
700	10.123		13.1	
800	10.126	10.128	13.3	13.3
800	10.127		13.5	

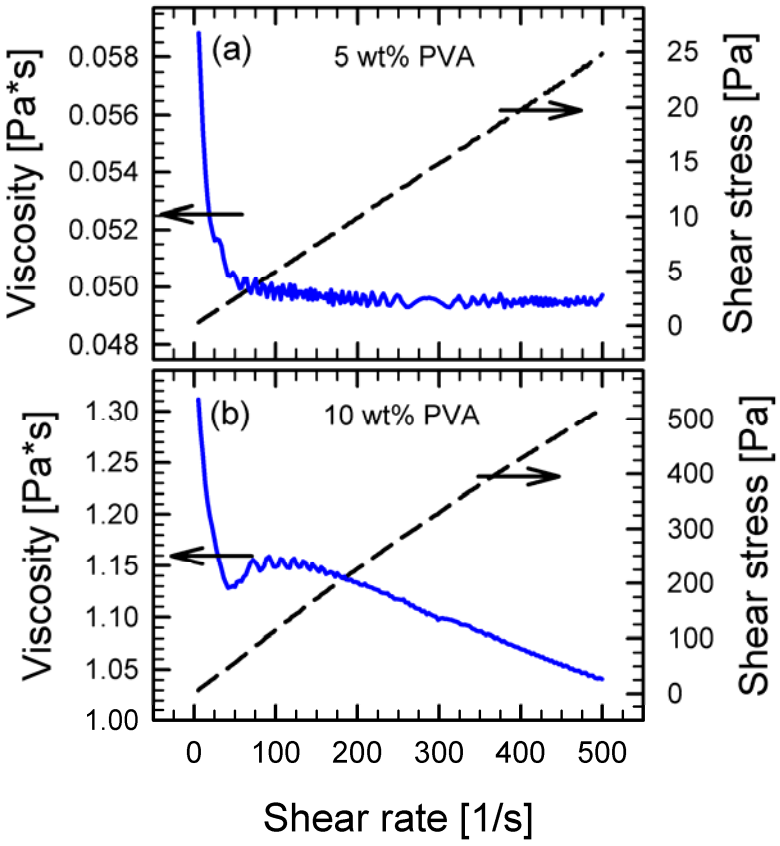

Figure 1. Viscosity (solid lines) and shear stress (broken lines) as a function of shear rate for solutions with 5 wt% (a) and 10 wt% PVA (b) dissolved in distilled water. The experiments were performed at 25 °C.

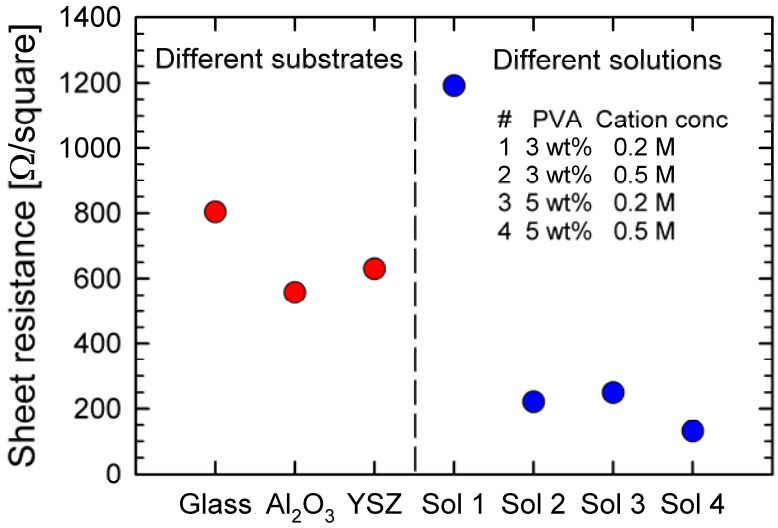

Figure 2. Sheet resistance of films prepared on different substrates and by using various solutions. The three films to the left were prepared from Solution 1, heat treated at 530 °C and deposited on glass, Al_2O_3 and YSZ substrates. The four films to the right were prepared from Solution 1 to 4, heat treated at 600 °C and deposited on Al_2O_3 substrates.

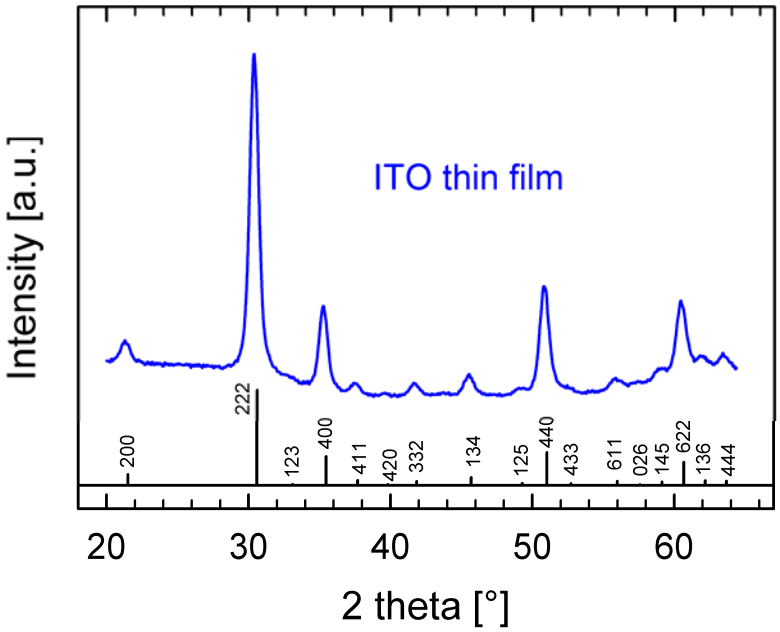

Figure 3. Gracing incident XRD pattern of an ITO thin film deposited on a YSZ substrate after heat treatment at 600 °C. The reference pattern for the cubic In_2O_3 bixbyite structure with space group $Ia\bar{3}$ is given at the bottom.

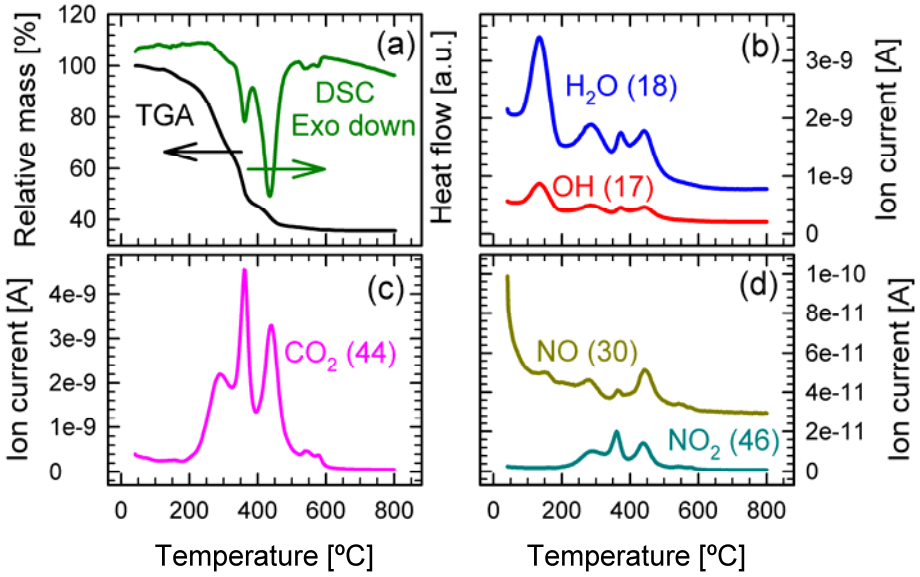

Figure 4. TGA and DSC of a gel prepared with tartaric acid and ethylene glycol as complexing agents (a), where the exhaust gases were analysed with a mass spectrometer (b, c and d). The atomic mass of the gas species is indicated.

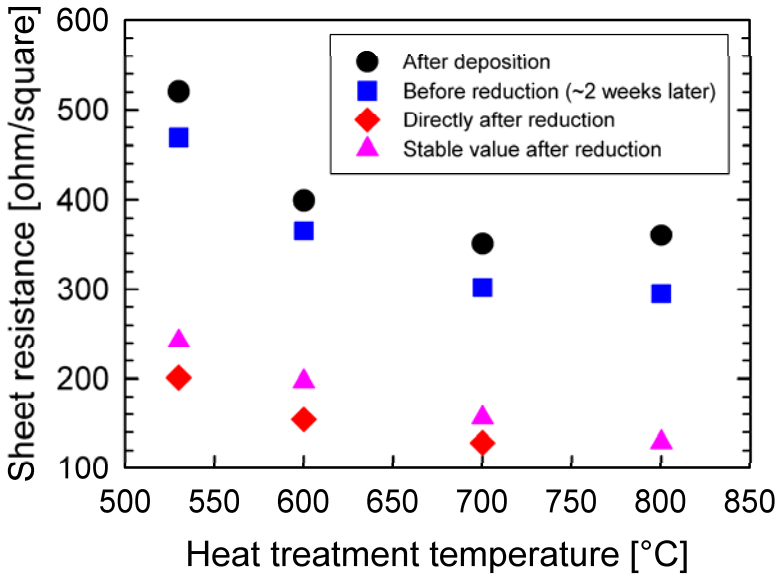

Figure 5. The sheet resistance after deposition, before the annealing performed about 2 weeks later, directly after the annealing and a few days after the annealing for ITO thin films deposited on YSZ.

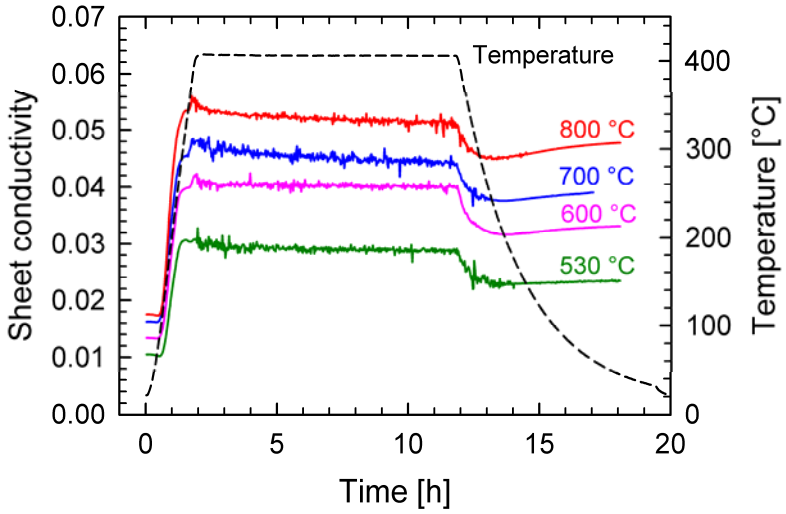

Figure 6. In situ conductivity of ITO films during annealing at 400 °C for 10 h in 5 % hydrogen in argon. The thin films were deposited on YSZ substrates and heat treated at temperatures ranging from 530 to 800 °C. The sheet conductivities and the temperature are given as solid lines and a broken line, respectively.

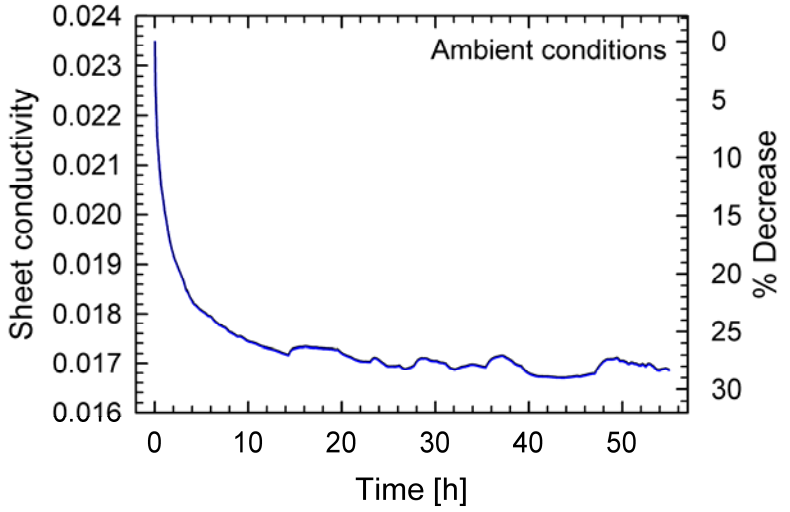

Figure 7. Ambient conductivity as a function of time for an ITO thin film on YSZ measured directly after the film was exposed to air after reduction. This film was heat treated at 530 °C. The variations in the conductivity after about 14 h could be related to temperature fluctuations inside the room during the time the experiment was performed.

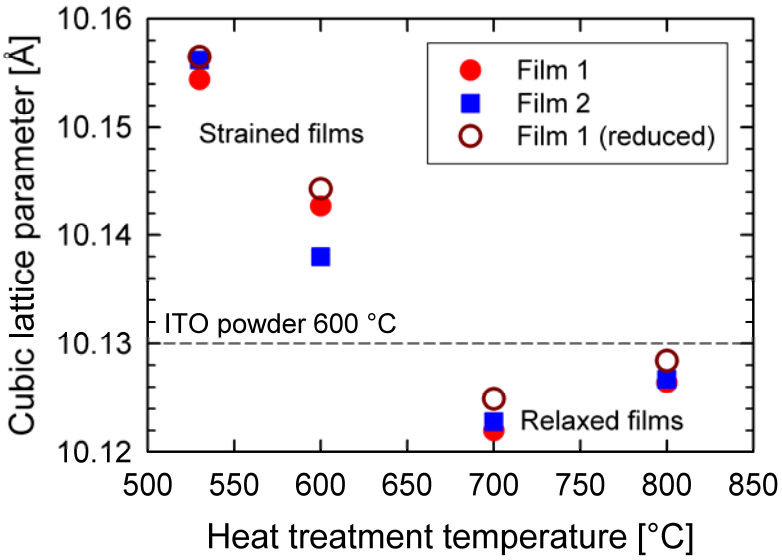

Figure 8. Cubic lattice parameter of ITO films deposited on YSZ substrates and heat treated at different temperatures before and after reduction for 10 h at 400 °C in 5 % hydrogen in argon. For comparison, the dashed line is the lattice parameter of ITO powder with the same composition after annealing at 600 °C [20].

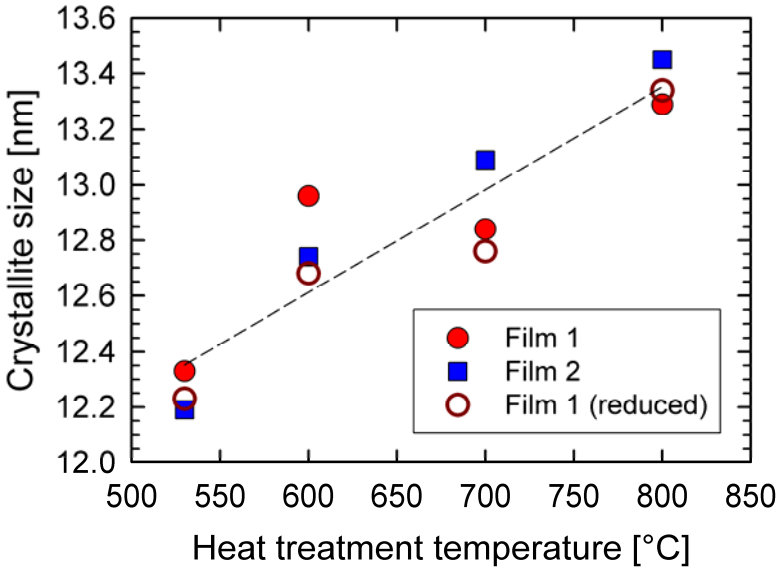

Figure 9. Crystallite size of ITO films deposited on YSZ and heat treated at different temperatures. The dashed line is a guide to the eye.

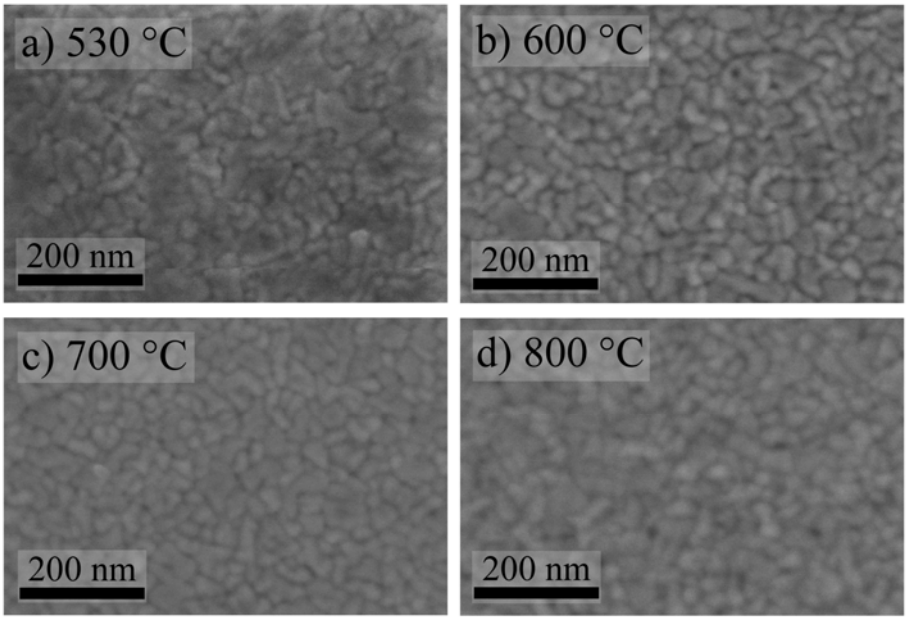

Figure 10. SEM micrographs of the top view of the surface of ITO thin films deposited on YSZ and heat treated at different temperatures.